Local enhancement of hydrogen production by the hydrolysis of Mg17Al12 with Mg “model” material

Serge Al Bacha, Eliana Desireé Farias, Philippe Garrigue, Mirvat Zakhour, Michel Nakhl, Jean-Louis Bobet, Dodzi Zigah

Local enhancement of hydrogen production by the hydrolysis of $Mg_{17}Al_{12}$ with Mg "model" material

S. Al Bacha[a,b,c,d], E. D. Farias[e], P. Garrigue[e], M. Zakhour[a], M. Nakhl[a], J.-L. Bobet[b*], D. Zigah[e,f*]

[a] LCPM/PR_2N (EDST), Lebanese University, Faculty of Sciences II, 90656 Jdeidet El Metn, Lebanon.

[b] University of Bordeaux, ICMCB, CNRS, UMR 5026, F-33600 Pessac, France.

[c] Institut de Chimie Moléculaire et des Matériaux d'Orsay (ICMMO) – ERIEE, UMR 8182 CNRS, Université Paris-Saclay, 91400, Orsay, France.

[d] Institut Lavoisier de Versailles, UMR 8180 CNRS, UVSQ, Université Paris-Saclay, 78035 Versailles Cedex, France.

[e] Univ. Bordeaux, CNRS UMR 5255, Bordeaux INP, ENSCBP, 33607 Pessac Cedex, France.

[f] Université de Poitiers, IC2MP UMR-CNRS 7285, 86073 Poitiers Cedex 9, France.

* corresponding authors: jean-louis.bobet@u-bordeaux.fr (J.-L. Bobet) and dodzi.zigah@univ-poitiers.fr (D. Zigah).

Highlights

- Galvanic coupling accelerates the corrosion of the unconventional cathode $Mg_{17}Al_{12}$.
- Detection of local flux of H_2 production from pure Mg and pure $Mg_{17}Al_{12}$ by SECM.
- Mg and $Mg_{17}Al_{12}$ in model Mg-$Mg_{17}Al_{12}$ show higher H_2 production.
- Hydrogen production by the hydrolysis reaction increases at the interface between Mg-$Mg_{17}Al_{12}$.

Abstract

The effect of galvanic coupling on the corrosion behavior of Mg and $Mg_{17}Al_{12}$ in Mg-Al alloys was studied by Scanning ElectroChemical Microscopy (SECM). The effect of galvanic coupling between Mg and $Mg_{17}Al_{12}$ was investigated using a "model" Mg+$Mg_{17}Al_{12}$ material with a controlled microstructure to evaluate the hydrogen evolution at a micrometric scale. SECM maps revealed that galvanic coupling between Mg and $Mg_{17}Al_{12}$ accelerates the corrosion rate (formation of a thicker passive layer) of both components. $Mg_{17}Al_{12}$ acts controversially to a

conventional cathode in galvanic system since hydrogen production by its hydrolysis reaction was found to increase due to the electron transfer with the anode (Mg).

Keywords: SECM, galvanic coupling, corrosion, Mg, $Mg_{17}Al_{12}$, hydrogen.

1. Introduction

The expend of magnesium (Mg) based materials used in many applications requiring lightweight materials (automotive, biomedical, technological, etc.) has shown many advantages [1,2]. Regarding the various applications of Mg-based alloys, their production continuously increases leading to a large accumulation of waste [3,4]. However, their recycling is not economically favorable [83, 84] since the processes (*e.g.* electrolytic (from $MgCl_2$) and thermal (reduction of MgO using graphite, Si, or Al)) are expensive [5,6]. In recent years, the production of hydrogen by hydrolysis reaction of metal and their hydrides (*e.g.* Mg/MgH_2 [7-12], $NaBH_4$ [13,14], $LiBH_4$ [15], …) attracts increased attention for its safety and its amenability to mild reaction conditions. Mg-based materials can be valorized by the hydrolysis reaction (corresponding to their corrosion where Mg is oxidized to Mg^{2+} and water is reduced to H_2 at normal conditions of pressure and temperature and without applying potential) in seawater (*i.e.* 0.6 mol/L NaCl) to produce the energy carrier H_2 [16-20].

AZ91 alloy ($Mg+Mg_{17}Al_{12}$) is one of the most common Mg alloys due to its low production cost, its good mechanical strength, and its corrosion resistance compared to pure Mg [21-25].
To better understand the corrosion (corresponding to the hydrogen production by the hydrolysis of Mg-based material) of AZ alloys, the behavior of each material, Mg and $Mg_{17}Al_{12}$ as well as their interaction must be revealed. The corrosion of Mg was reported in previous studies [21, 26-28] and the effect of $Mg_{17}Al_{12}$ on the corrosion mechanism of Mg-Al alloys has been previously discussed where it has been shown that the intermetallic may act as a cathode (accelerating Mg corrosion) or as a corrosion barrier (improving Mg corrosion resistance) [29-39].
This paper discusses the effect of the interaction between Mg and $Mg_{17}Al_{12}$ and their behavior during the corrosion process. Previous studies on the corrosion behavior of pure $Mg_{17}Al_{12}$ in NaCl solution (where Cl^- anions favor the formation of water-soluble $MgCl_2$ inhibiting the formation of $Mg(OH)_2$ passive layer) [40,41] confirmed that a galvanic coupling between Mg and $Mg_{17}Al_{12}$ exist and that “global” corrosion of $Mg_{17}Al_{12}$ is slower than that of Mg. The effect of the galvanic coupling between these two phases was studied indirectly through several AZ91 model materials where the microstructures of the materials can be controlled. The change in the corrosion rate of Mg was attributed to the galvanic coupling between Mg and $Mg_{17}Al_{12}$ [42].

The local corrosion behavior of magnesium alloys has been studied using local probe techniques, providing microscopic information on electrochemical processes occurring locally on the surface. These techniques (*e.g.* localized electrochemical impedance spectroscopy [43,44], scanning vibrating electrode technique [45], Kelvin probe force microscopy [46]) can measure currents and/or potentials with high spatial resolution, to elucidate differences in electrochemical behavior between different components on the same surface [47]. However, SECM has the ability to measure the current based on a faradic reaction at a microelectrode. This technique encompasses a wide variety of modes (feedback, generation/collection, redox competition, direct and potentiometric) which provide information on local electrochemical activity and/or surface topography on a micrometric scale [48-51]. Because of its high reactivity in water, studying the corrosion of magnesium-based materials by SECM is challenging [47,52].

In this study, the hydrogen evolution reaction on pure Mg, pure $Mg_{17}Al_{12}$ and Mg+$Mg_{17}Al_{12}$ model material (with a similar composition of AZ91 alloy but a different microstructure) was investigated locally through SECM. This original microstructure allows us to better identify each material during the SECM imaging. Also by comparing the corrosion behavior of the same Mg and $Mg_{17}Al_{12}$ powders as pure phases and when in contact in an AZ91 alloy, the effect of galvanic coupling on the hydrogen production performances can be revealed. In fact, the use of a "model" Mg+$Mg_{17}Al_{12}$ synthesized by mixing pure Mg and $Mg_{17}Al_{12}$ offer the advantage (i) to control the composition of each phase (*e.g.* second phase in AZ alloys is usually a mix Mg and $Mg_{17}Al_{12}$ while in the model material the second phase is pure $Mg_{17}Al_{12}$), (ii) to be able to compare the corrosion behavior of pure Mg and $Mg_{17}Al_{12}$ and the same Mg and $Mg_{17}Al_{12}$ in the alloy and (iii) to reduce the effect of particle size on the hydrolysis performance [53] of the model material (conserving the same particle size in the model material as those in each pure material).

The vertical tip-substrate distance was first adjusted through Z-approach curves using feedback mode in an absolute ethanol solution while the electrochemical reactivity of the surface was investigated by collecting the generated H_2 in NaCl solution. Measurements carried out on pure Mg and pure $Mg_{17}Al_{12}$ confirmed the previously reported results on the corrosion of each of the two materials [41,42,54]. The effect of galvanic coupling on the corrosion behavior of both Mg and $Mg_{17}Al_{12}$ was clarified through SECM mapping of "Mg+$Mg_{17}Al_{12}$" material with the same composition of AZ91 (apart from the presence of 1 wt.% of Zn) but with a controlled microstructure [42]. Our findings allow to better understand the effect of galvanic coupling on the corrosion of both Mg and $Mg_{17}Al_{12}$.

2. Experimental details

2.1. Materials and samples preparation

The studied materials are pellets, with an exposed surface of 0.8 cm^2, manufactured by cold-pressing of magnesium powder (Strem Chemicals, 99.8%), homemade $Mg_{17}Al_{12}$ [55] and a $Mg+Mg_{17}Al_{12}$ powder (corresponding to "$Mg+Mg_{17}Al_{12}$ fusion" in reference [42]). Pure $Mg_{17}Al_{12}$ was prepared by melting 56 wt.% of Mg with 44 wt.% of Al under inert atmosphere (*i.e.* Ar) at 813K for 8h followed by a sintering at 725K for 18h and cooling-down to ambient temperature normally [55]. $Mg+Mg_{17}Al_{12}$ was prepared by melting 78 wt.% of pure Mg with 21 wt.% of pure $Mg_{17}Al_{12}$ (to facilitate the identification of both phases at glance during the positioning of the UME during SECM measurements) following the same process adopted for the synthesis of pure $Mg_{17}Al_{12}$ [42]. XRD patterns and elemental composition of the materials involved in this study are presented in Supplementary materials Figures S1 and S2 respectively. The specimens were abraded with SiC paper from 600 to 4000 grit in absolute ethanol consecutively. Experiments were performed in 60 mmol/L NaCl (UNI-CHEM, 99.8%) prepared in ultrapure distilled water (18.2 MΩ.cm). The concentration of NaCl is 10 times less concentrated than the average concentration of NaCl in seawater (*i.e.* 0.6 mol/L) to reduce the corrosion rate (consequently the surface evolution and intense hydrogen bubbles formation) while retaining the effect of chloride ions.

2.2. Microstructural analysis

The microstructure of $Mg+Mg_{17}Al_{12}$ was analyzed using a TESCAN VEGA3 SB microscope equipped with a backscattered electron detector (BSE) and an energy dispersive X-ray spectrometer (QUANTAX EDS from Bruker) for the identification of both phases. Optical micrographs before and after tests were acquired using a Leica Z16 APO microscope.

2.3. SECM setup

All electrochemical measurements were performed using the SECM, CHI920C from CH Instruments, Inc. The instrument is equipped with an adjustable stage for tilt correction. It was used in a typical three electrode configuration; the substrate was unbiased. The cell was made from Teflon with an opening of 0.2 cm^2 in the middle into which the sample was tightly fitted. The tip was a homemade Pt disk ultramicroelectrode (UME) with a radius (a) of 12.5 µm and an RG ≈ 7. The Pt UME was used as the working electrode, a Pt wire as the auxiliary electrode and an Ag/AgCl/NaCl 3 mol/L as the reference electrode. The sample was left at open circuit potential during experiments.

Line scan experiments were performed in the x-direction over a distance of 500 µm every 5 minutes after immersion in 60 mmol/L NaCl solution with a scan rate of 10 $\mu m.s^{-1}$. SECM images were gathered as the tip was moved by the stepper controller over the sample surface (500 µm × 500 µm) with a scan rate of 100 $\mu m.s^{-1}$. This scan rate was chosen to limit the surface evolution between the start and the end of the measurement. The entire scanning time was approximately 22 minutes. All experiments were carried out in a Faraday cage at room temperature.

3. Results and discussion

During SECM measurements using an amperometric probe [50], the recorded current, resulting from the collection of redox species, depends on the sample surface electrochemical reactivity and the distance between the probe and the sample [56]. In order to improve the collection efficiency of the tip, a small distance between the tip and the substrate should be achieved (L<2) [57]. Nowadays, SECM can be coupled with an optical microscope to adjust the distance L [58] or with a shear force system [59]. Considering that this combination is not always available, the feedback mode was used to control the tip-substrate distance.

The positioning of the tip above the surface was achieved by locating defects on the surface of $Mg+Mg_{17}Al_{12}$. These defects were visible at a glance (Figure 1).

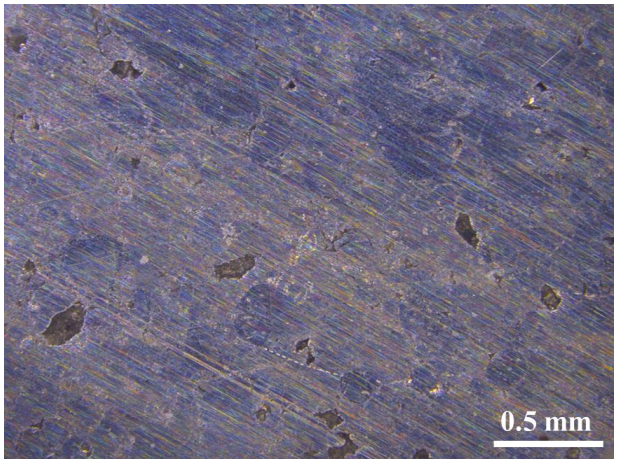

Figure 1: Optical micrographs of $Mg+Mg_{17}Al_{12}$ surface before immersion in 60 mmol/L NaCl solution.

3.1. Tip-substrate distance control

Mg-based material (Mg and $Mg_{17}Al_{12}$, *Cf* reactions (1) and (2) respectively) reacts with the aqueous NaCl solution to produce H_2 and a hydroxide by-product [55].

$$Mg + 2\,H_2O \rightarrow Mg(OH)_2 + H_2 \quad (1)$$

$$Mg_{17}Al_{12} + 58\,H_2O \rightarrow 17\,Mg(OH)_2 + 8\,Al(OH)_3 + 4\,Al^{11} + 29\,H_2 \quad (2)$$

Generated hydrogen, during the corrosion of Mg and/or $Mg_{17}Al_{12}$, is an electroactive species that can be oxidized at the Pt UME following reaction (3) (figure 2.a):

$$H_2 \rightarrow 2\,H^+ + 2\,e^- \quad (3)$$

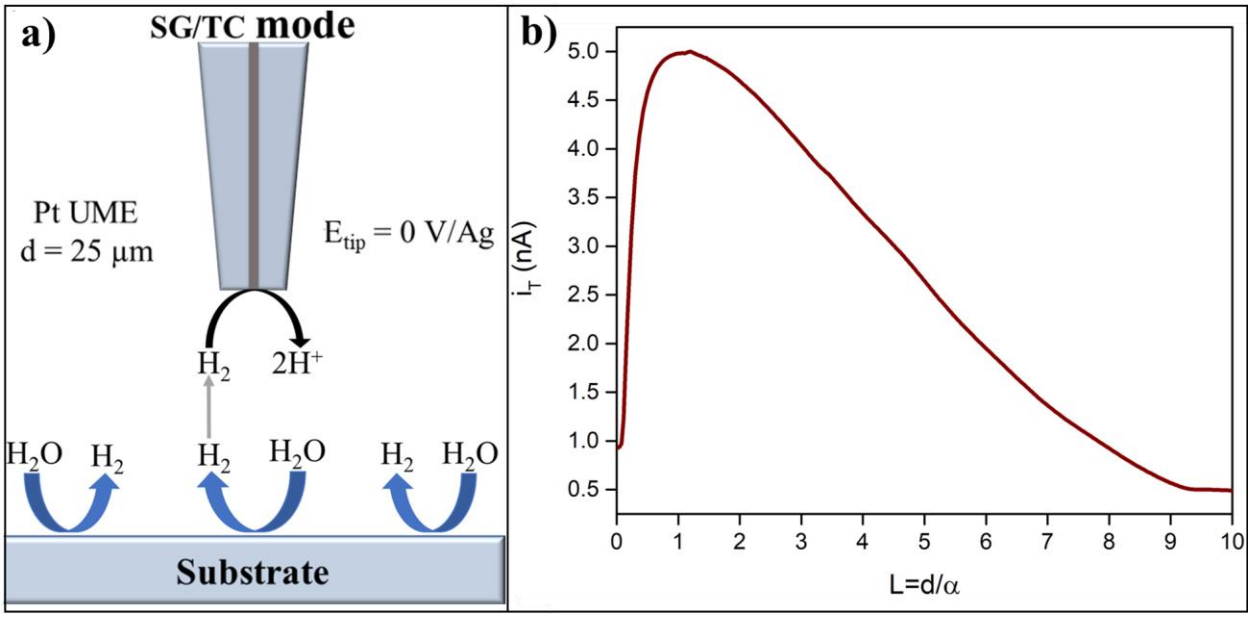

Figure 2: a) SECM experiment on a 25 µm Pt UME using SG/TC mode for the detection of hydrogen, E_{tip} = 0 V/Ag and b) the approach curve recorded above $Mg_{17}Al_{12}$ surface using SG/TC mode with detection of H_2. Tip radius = 12.5 µm, approach rate = 1 µm.s^{-1}.

Figure 2.b shows the approach curve above on the less reactive material $Mg_{17}Al_{12}$ surface [42] in 60 mmol/L NaCl solution monitoring the flux of the generated H_2 (the same approach curves are presented using micron scale in Supplementary materials Figure S3). The measured current i_T, proportional to the concentration of H_2 in the medium, increase when the dimensionless factor

[11] Al is covered by a protective $Al(OH)_3$ layer preventing its hydrolysis in "extreme" hydrolysis solutions (*e.g.* 0.5M HCl).

L ($L = \frac{d}{\alpha}$, with *d* the tip-substrate distance and *α* the tip radius) with decreases from 10 to 1 as expected due to the formation of H_2 on the substrate. Nevertheless, the current gradually decreases for L<1, indicating lower H_2 concentration when the tip is closer to the substrate. Consequently, the determination of the tip-to-substrate distance by the collection of hydrogen in SG/TC mode is not straightforward and may differ according to the corrosion behavior of the sample, in this case it is not clear if L = 0 is really the surface of our substrate. The poor reproducibility of the curves obtained in SG/TC mode, and the difficulty in determining the surface of the substrate, led us to use the feedback mode to control the distance between the tip and the substrate.

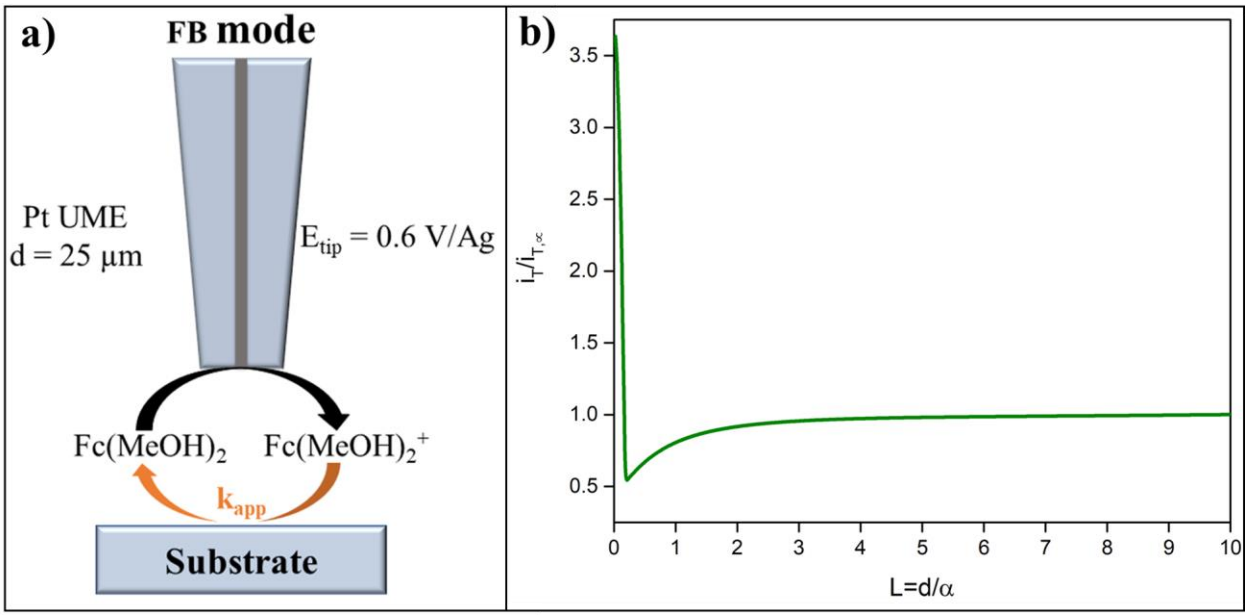

Figure 3: a) SECM experiment on a 25 µm Pt UME using Feedback mode in 1 mmol/L of $Fc(MeOH)_2$ in ethanol, E_{tip} = 0.6 V/Ag and b) the approach curve recorded above $Mg_{17}Al_{12}$ surface using Feedback mode with $Fc(MeOH)_2$ as mediator at 1 mmol/L in ethanol, E_{tip}= 0.6 V/Ag. Tip radius = 12.5 µm, approach rate = 1 µm.s^{-1}.

$Fc(MeOH)_2$ was used as a mediator in an absolute ethanol solution for the approach curve in feedback mode (Figure 3) since the corrosion rate of Mg in pure ethanol is much slower than in pure H_2O or in NaCl aqueous solution [60,61]. Lowering the corrosion rate of the substrate during the SECM adjustment is necessary to decrease the hydrogen evolution since its generation will disturb the steay state current due to the oxidation of $Fc(MeOH)_2$. Indeed, at E_{tip} = 0.6 V, the potential applied to oxidize the $Fc(MeOH)_2$, H_2 can also be oxidized, and the current measured at the tip is proportional to both the concentration and the diffusion coefficient of the electroactive species. Figure 3.b shows the approach curve on $Mg_{17}Al_{12}$ surface in 1 mmol/L $Fc(MeOH)_2$ solution. A typical approach curve represents the normalized current, $I_T = i_T/i_{T,\infty}$ (tip

current/steady state current) in function of the normalized distance L. The calculated [62] steady state current $i_{T,\infty}$ was 3.0 nA while the experimental value of $i_{T,\infty}$ was in the range of 2.7 nA to 3.0 nA. Since $i_{T,\infty}$ is almost constant regardless the substrate composition as shown in Supplementary materials Figure S5, we can conclude that the substrate does not affect the composition of the $Fc(MeOH)_2$ solution.

When the tip is positioned close to the surface ($0.1 < L < 1$, *Cf* Figure 1.b), i_T is lower than $i_{T,\infty}$ indicating that the surface has an intermediate behavior that tends to the negative probe approach curve. This result indicates that the Mg alloy is covered by an oxide layer (*i.e.* corresponding to the passivation layer [63]) that hinders the diffusion of the mediator. However, the pure negative FB behavior, that can be obtained for example on a Teflon surface (Figure S6), is not reached. This result indicates that the $Fc(MeOH)_2^+$ can penetrate inside the oxide layer to react with metallic layer below, which means that the oxide is porous [64,65]. In fact, corrosion of Mg-based materials occurs in ethanol with a lower corrosion rate as mentioned above. However, it was not possible to observe a fast electron transfer between the mediator and the substrate and the current did not increase when the distance between the tip approaches near the surface. At lower L ($L < 0.1$), the tip seems in direct contact with the conductive $Mg_{17}Al_{12}$ and an increase of the current is observed in Figure 3.b. For more details about the adjustment of the tip to substrate distance, the reader can refer to the supplementary materials section "SECM using feedback mode".

3.2. Hydrogen generation

The working distance of the UME tip above the surface was set to 20 µm (L=1.6) for the reasons mentioned below:

(i) for optimum collection efficiency of the tip, L is recommended to be lower than 2 [57].

(ii) the oxidation reaction of hydrogen at the tip generates H^+ ions which lower the pH and favors the dissolution of the passivation layer (following the Henderson-Hasselbalch equation [55]). This favors the oxidation of unreacted Mg and therefore, the current modification is attributed to the destabilization of the passivation layer. Hence the tip should not be too close to the substrate so that the effect of H^+ ions will be less pronounced (figure 2.a).

(iii) the formation of the passivation layer can reduce the distance between the tip and the surface. Keeping the tip at L = 1.6, allow us to avoid any damage to the tip.

Hydrogen evolution (*e.g.* hydrogen collection, …) is one of the most efficient methods of measuring the corrosion rate of magnesium and its alloys in aqueous media [16-18,42]. Using SECM in SG/TC mode presents an alternative way of studying the corrosion rate by collecting hydrogen at the tip (Figure 2.a). After the approach curves measurements and the positioning of the tip, the $Fc(MeOH)_2$ solution was replaced by a 60 mmol/L NaCl solution to investigate the corrosion behavior of the samples by SG/TC mode by collecting the generated H_2.

3.3. Interaction between Mg and $Mg_{17}Al_{12}$

SECM has shown great potential to map the corrosion process in heterogeneous materials [66]. In order to investigate the electrochemical interaction between Mg and $Mg_{17}Al_{12}$, SECM maps were carried out in 60 mmol/L NaCl solution.

Figures 4.a and 4.b show the SEM micrographs with BSE detector and EDS mapping respectively. The yellow zone in Figure 6.b corresponds to $Mg_{17}Al_{12}$ while Mg appears red. The area of interest of 500 µm × 500 µm is delimited by the white square on Figures 4.a and 4.b. However, the measured surface during immersion may deviated and the overlay of the SECM and the micrograph is complicated since the surface evolves even in low conductivity (1 mmol/L $Fc(MeOH)_2$ in ethanol) solution.

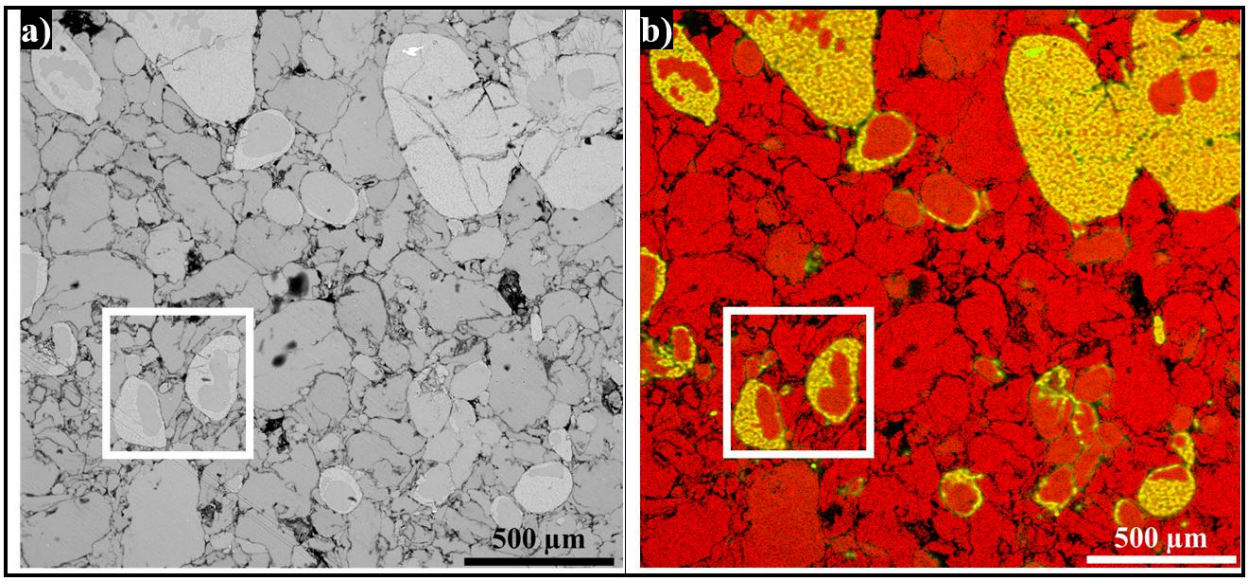

Figure 4: SEM image with a) BSE detector and b) EDS detector of the surface of $Mg+Mg_{17}Al_{12}$. The area of interest (500 µm × 500 µm) is delimited in the white square.

3.3.1. Surface mapping in NaCl solution

SECM mapping was carried out without applying any voltage. Higher i_T reflects higher H_2 production hence higher corrosion reactivity while lower i_T is indicative of either unreacted surface or passivated surface. To distinguish between the latter cases, the maps were collected successively after 1 min (Figure 5.a) and 23 min (Figure 5.b).

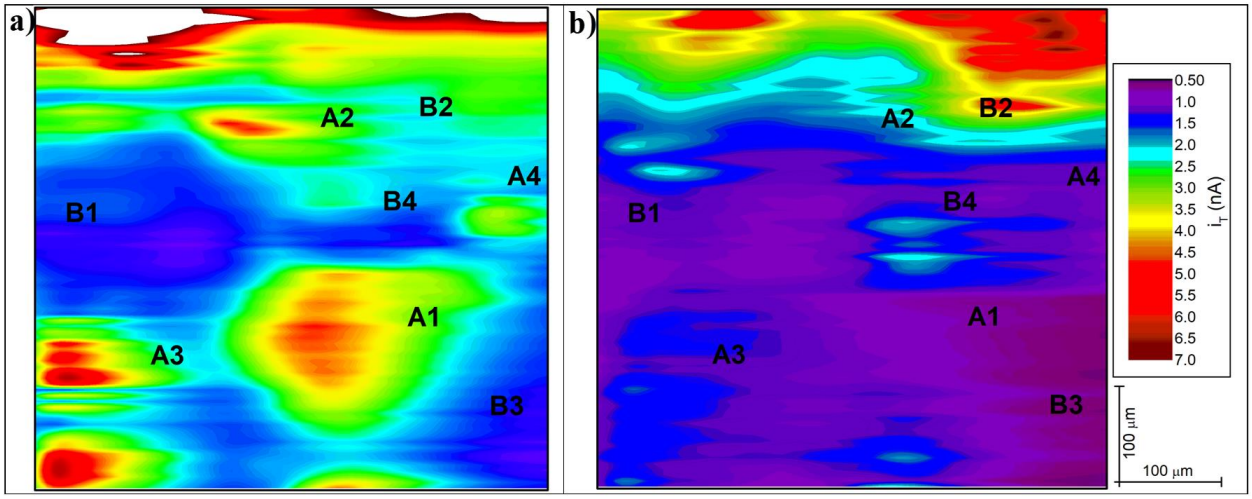

Figure 5: Hydrogen evolution maps of Mg+$Mg_{17}Al_{12}$ acquired by SG/TC mode without applying any voltage after a) 1 min and b) 23 min of immersion in NaCl 60 mmol/L. Scan rate = 100 µm.s^{-1} and acquisition time for each image = 22 minutes.

The contrast observed in Figures 5.a and 5.b shows the difference in the reactivity between surface components. i_T varies in a wide range (*e.g.* 27-1.2 nA when immersed for 5 minutes) due to the presence of different materials with different corrosion reactivities (the "global| corrosion kinetics of pure Mg is higher than pure $Mg_{17}Al_{12}$ [42]). After 23 minutes of immersion (Figure 5.b), the corrosion reactivity of Mg+$Mg_{17}Al_{12}$ decreased due to the formation of the passivation film on the surface.

The evolution of the surface was investigated by comparing Figures 5.a and 5.b to identify Mg and $Mg_{17}Al_{12}$. Pure Mg corrodes faster than pure $Mg_{17}Al_{12}$ as reported in references [41,42,55]. This will induce the formation of an oxide layer on Mg much faster than on $Mg_{17}Al_{12}$. As a consequence, for Mg, i_T will significantly decrease between both figures while it increases or varies slightly for $Mg_{17}Al_{12}$. Based on this reasoning, Mg zones were marked as "A1, A2, A3 and A4" and $Mg_{17}Al_{12}$ zones were marked as "B1, B2, B3 and B4" on Figures 5.a and 5.b. We were obliged to use this reasoning because it was not possible to match the SEM image with the image obtained by SECM.

The main variance between Mg and $Mg_{17}Al_{12}$, in the alloy, is their spatial reactivity where the current recorded above Mg is minimal at the Mg-$Mg_{17}Al_{12}$ interface while it is maximal at the interface for $Mg_{17}Al_{12}$. The galvanic coupling between Mg and $Mg_{17}Al_{12}$ increases their corrosion at their interface:

- This effect is noticeable for $Mg_{17}Al_{12}$ (*e.g.* zone "B4") where the current is maximal at the interface between Mg and $Mg_{17}Al_{12}$ in Figure 5.a while it becomes minimal in the same region as shown in Figure 5.b. Moreover, zone "B3" shows that, for $Mg_{17}Al_{12}$, the hydrogen production is higher at the interface.
- For Mg, considering its corrosion rate, the interface is rapidly passivated (i_T decreases) resulting in lower current at the interface. The current recorded above the zone "A1" decreases from 6.0 nA to 0.8 nA with a maximal current above the interface while carrying out the second SECM map (Figure 5.b).

The higher corrosion rate at the interface is attributed to the electronic transfer between the anode (Mg with E_{OCP} (Mg) = -1.65 V/SCE [54]) and the cathode ($Mg_{17}Al_{12}$ with E_{OCP} ($Mg_{17}Al_{12}$) = -1.2 V/SCE [41]) and to the surface defects (*e.g.* grain boundaries, cracks, …) that acts as corrosion initiator sites [67]. The passivation of Mg when it is in contact with $Mg_{17}Al_{12}$ is favored.

The overlay of SECM maps and SEM images is necessary in the corrosion investigation by SECM. However, optical micrographs of Mg+$Mg_{17}Al_{12}$ after SECM measurements (Figures 6) show the surface evolution which complicates the overlay of SECM results with morphological analysis (scanning electron microscopy and optical microscopy images).

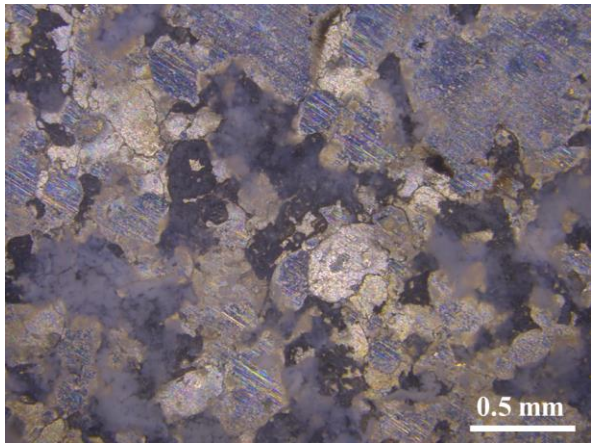

Figure 6: Optical micrographs of Mg+$Mg_{17}Al_{12}$ surface after immersion in 60 mmol/L NaCl solution.

3.3.2. Comparison with pure materials

In an attempt to reveal the effect of galvanic coupling on the corrosion (consequently hydrogen production) of Mg and $Mg_{17}Al_{12}$ in the model material, current was recorded along the same line every 5 minutes above pure Mg and pure $Mg_{17}Al_{12}$ (*i.e.* the same materials used for the synthesis of the model material) for better comparison. The measurements were acquired without applying any voltage (at their OCP), the samples were scanned in x direction, at a constant distance of 20 µm, for 500 µm.

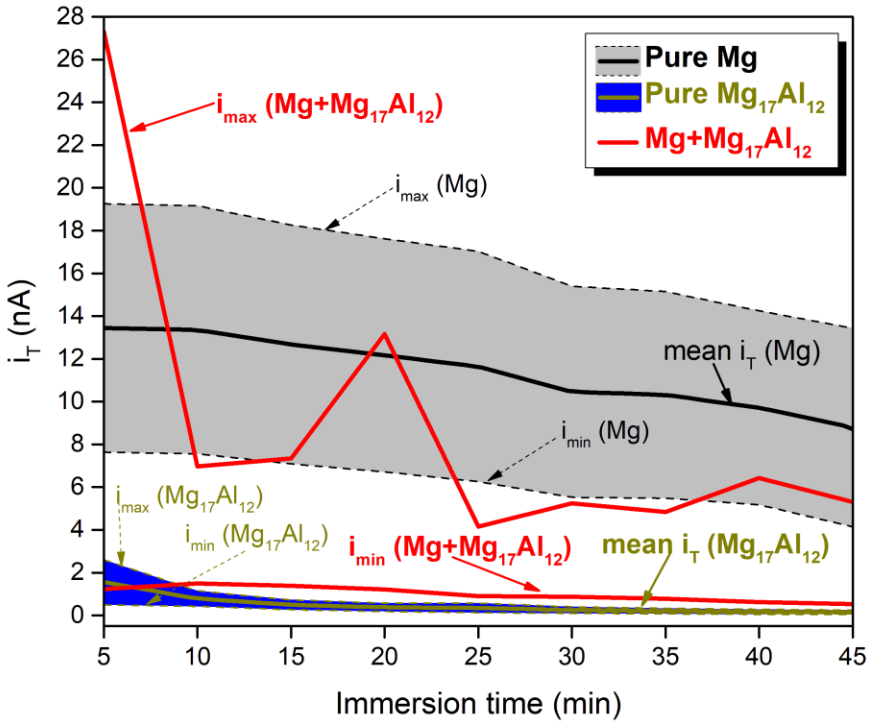

Figure 7: Variation of the measured current i_T in SG/TC mode using the generated H_2 for pure Mg, pure $Mg_{17}Al_{12}$, and Mg+$Mg_{17}Al_{12}$ with immersion time in 60 mmol/L NaCl solution.

Figure 7 shows the mean current i_T calculated by averaging the results from each line scan, every five minutes. These measurements were repeated at least thrice. An example of the line scan recorded after 5 minutes and 25 minutes of immersion in NaCl solution is presented in Supplementary materials Figure S4. This calculation allows us to reduce the impact of the inhomogeneity on the surface to be able to compare the samples. However, as the current measured at each time represents the average on the line, it allows us to have an order of magnitude on the average reactivity of the surface. The variation of i_T values during SECM maps acquisition (Figures 5.a and 5.b) are presented as i_{max}(Mg+$Mg_{17}Al_{12}$) and i_{min}(Mg+$Mg_{17}Al_{12}$) in Figure 7 to compare the corrosion behavior of Mg and $Mg_{17}Al_{12}$ in the model material to pure Mg

and pure $Mg_{17}Al_{12}$. The values from 5 to 20 minutes correspond to the first map (Figure 5.a) while the values from 25 to 45 minutes correspond to the second map (Figure 5.b).

Scanning above $Mg_{17}Al_{12,}$ after 5 min in the corrosive solution, the average current measured is around 1.6 nA. This low current indicates a low production of H_2 on the material compared to pure Mg where the current start at 14.7 nA. This value is around 10 times higher than that reached for $Mg_{17}Al_{12}$. This high difference between the two surfaces allows us to conclude that a high production of H_2 is stretched above Mg, as expected. This current decreases with time in both cases, suggesting the formation of the passivation layer that slow down the production of H_2 as previously reported [68]. Above $Mg_{17}Al_{12}$ the production of H_2 is almost stopped. Comparing the values of i_T recorded above pure Mg and pure $Mg_{17}Al_{12}$ to those measured during the SECM map acquisition (Figure 5), the Mg+$Mg_{17}Al_{12}$ has the higher current at the beginning of the experiment. This result suggests that the combination of the two materials induces a higher generation of H_2 which implies a higher corrosion reactivity. Nevertheless, the value of the current is of the same order of magnitude that the one for Mg. However, the current decreases faster on Mg+$Mg_{17}Al_{12}$ than above Mg confirming the higher corrosion rate when the galvanic coupling is established. Hydrogen collection decreases by prolonging the immersion time in NaCl solution for pure Mg, pure $Mg_{17}Al_{12}$ and Mg+$Mg_{17}Al_{12}$ in total agreement with previous observations [40,42]. The corrosion is interrupted by the formation of an inhomogeneous passivation layer of solid $MgO/Mg(OH)_2$ on the surface [63] which inhibits the reaction between water and Mg/$Mg_{17}Al_{12}$ thus limiting the hydrogen production [69]. The current above Mg+$Mg_{17}Al_{12}$ becomes lower than Mg due to the faster formation of the passivation layer, implying higher initial corrosion reactivity.

The variation of i_T extracted from SECM mapping results is represented for comparison between Mg and $Mg_{17}Al_{12}$ (*i.e.* i_{max} and i_{min}, *Cf* Figure 7). These results should be taken with caution because the surface scanned in SECM is not homogeneous. The gap between i_{max} and i_{min} is related to the non-uniform corrosion of Mg and $Mg_{17}Al_{12}$ [28]. After 5 minutes of immersion in NaCl solution, the current varies in the range 19.3 – 10.5 nA, 2.6 – 0.54 nA and 27.3 – 1.2 nA for pure Mg, pure $Mg_{17}Al_{12}$ and Mg+$Mg_{17}Al_{12}$ respectively (Figure 7). The greater difference between i_{max} and i_{min} for Mg+$Mg_{17}Al_{12}$ (*i.e.* 27.3 – 1.2 nA) is attributed to the heterogeneous composition of the surface (Mg and $Mg_{17}Al_{12}$). i_{min} (Mg+$Mg_{17}Al_{12}$) is higher than i_{max} ($Mg_{17}Al_{12}$) while i_{max} (Mg+$Mg_{17}Al_{12}$) is greater than i_{max} (Mg) after 5 min of immersion in NaCl solution. These results show that the galvanic coupling established between Mg and $Mg_{17}Al_{12}$ accelerates H_2 production by the hydrolysis (*i.e.* corrosion) of both materials in contradiction with previous studies stating that galvanic coupling is not significant between both materials [31]. By definition, galvanic coupling favors the oxidation of the less noble material (Mg) while it lowers the one of the more noble ($Mg_{17}Al_{12}$) [70]. Note that $Mg_{17}Al_{12}$ in Mg-Al alloys can behave simultaneously as an anode (reaction 2) and a cathode (ΔE ($Mg_{17}Al_{12}$–Mg) > 250 mV considered for galvanic coupling [54]

which accelerates the corrosion of the anode Mg [41,71]). For the latter reasons, $Mg_{17}Al_{12}$ is considered as an “unconventional cathode” in Mg-Al alloys (*e.g.* AZ alloys).

Our results indicate that, in Mg-Al alloys, the galvanic coupling between Mg and $Mg_{17}Al_{12}$ accelerates H_2 production (*i.e.* corrosion) from both the anode (Mg) and the unconventional cathode ($Mg_{17}Al_{12}$).

4. Conclusions

The present study demonstrates the efficiency of the scanning electrochemical microscopy to investigate the corrosion of Mg-based materials by standard equipment (without optical devices). Approach curves were carried out by feedback mode in 1 mmol/L $Fc(MeOH)_2$ in absolute ethanol to decelerate the corrosion of Mg-based materials before performing the corrosion measurements in NaCl solution to keep the same tip-to-substrate distance. The local corrosion behavior was investigated by SG/TC mode using the generated H_2. Our method was used to study the galvanic coupling of Mg and $Mg_{17}Al_{12}$ at the micrometric scale.

Hydrogen collection in SG/TC SECM mode is an efficient method to investigate the corrosion behavior of heterogeneous Mg-based materials surface. Hydrogen production decreases when prolonging immersion time in NaCl due to the formation of the protective passivation layer. The current recorded above pure Mg and pure $Mg_{17}Al_{12}$ were taken as references to distinguish the effect of galvanic coupling between both materials. Monitoring the hydrogen production above the surface of Mg+$Mg_{17}Al_{12}$ shows that the reactivity of pure $Mg_{17}Al_{12}$ is lower than that of $Mg_{17}Al_{12}$ in contact with Mg. This suggests that galvanic coupling in Mg-Al alloys not only promotes corrosion of the less noble material (*i.e.* Mg) but also the corrosion of the more noble material ($Mg_{17}Al_{12}$). Local corrosion measurements map the hydrogen production at the interface between Mg-$Mg_{17}Al_{12}$. Above $Mg_{17}Al_{12}$, higher reactivity is recorded at the interface while the reactivity was maximal above the surface of Mg. The corrosion rate of Mg increases owing to galvanic coupling; hence Mg corrodes faster at the interface Mg-$Mg_{17}Al_{12}$, resulting in rapid formation of a passivation layer. This results in recording a lower current for Mg above the Mg-$Mg_{17}Al_{12}$ interface, instead of measuring the highest current above the same region. Nevertheless, this phenomenon is observed above $Mg_{17}Al_{12}$ due to its low corrosion rate.

In conclusion, the present investigation showed that galvanic coupling increases the corrosion rate of the unconventional cathode (anode and cathode simultaneously) in Mg-Al alloys. We anticipate that these findings will offer better understanding of the galvanic coupling between

Mg and $Mg_{17}Al_{12}$ in Mg-Al alloys and of the effect of $Mg_{17}Al_{12}$ on the corrosion mechanism of the alloy.

Acknowledgments

This work was financially supported by the AZM & SAADE Association, the Lebanese University (Scientific research support program) and Bordeaux foundation. This work was partially funded and performed within the framework of the Labex AMADEUS ANR-10-LABEX-0042-AMADEUS with the help of the French state Initiative d'Excellence IdEx ANR-10-IDEX-003-02.

Local enhancement of hydrogen production by the hydrolysis of $Mg_{17}Al_{12}$ with Mg "model" material

S. Al Bacha, E. D. Farias, P. Garrigue, M. Zakhour, M. Nakhl, J.-L. Bobet, D. Zigah.

Supplementary materials

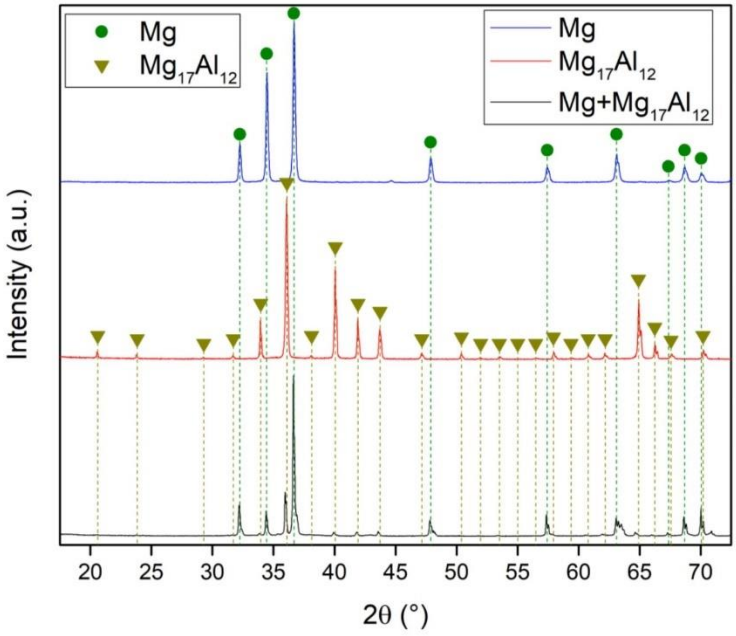

Figure S1: XRD patterns of pure Mg, pure $Mg_{17}Al_{12}$ and the model material $Mg+Mg_{17}Al_{12}$.

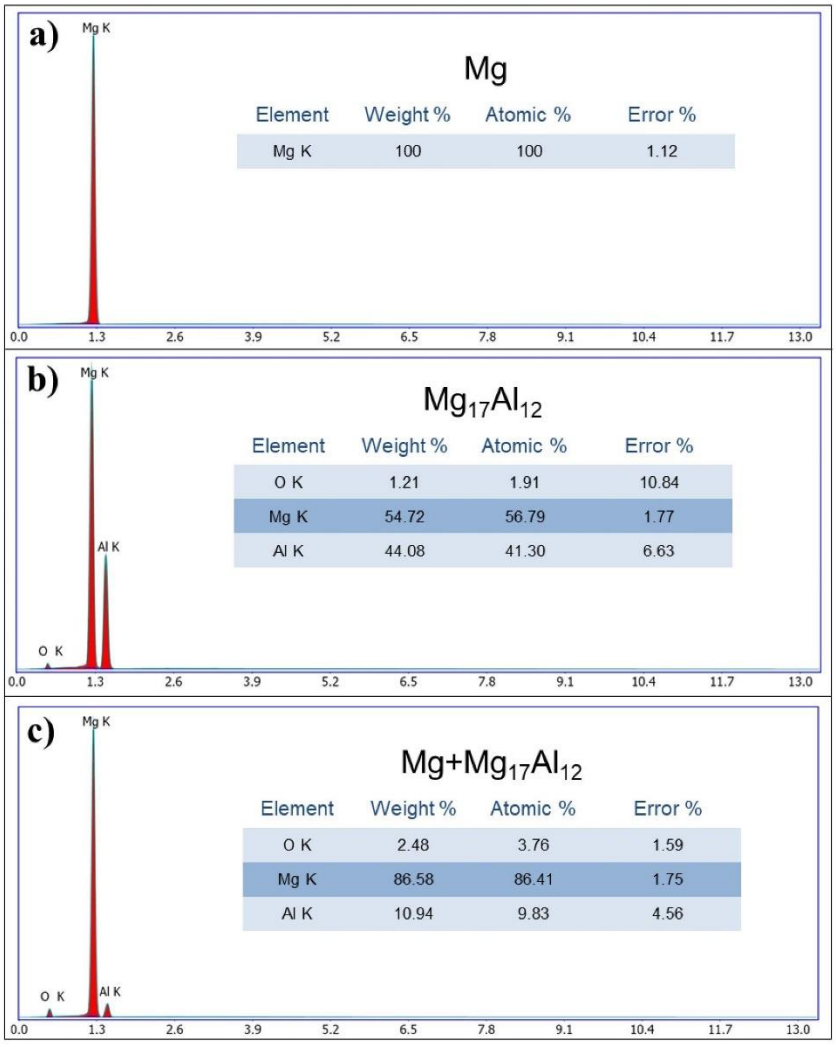

Figure S2: Elemental composition of the surface of a) pure Mg, b) pure $Mg_{17}Al_{12}$ and c) $Mg+Mg_{17}Al_{12}$ evaluated by EDS.

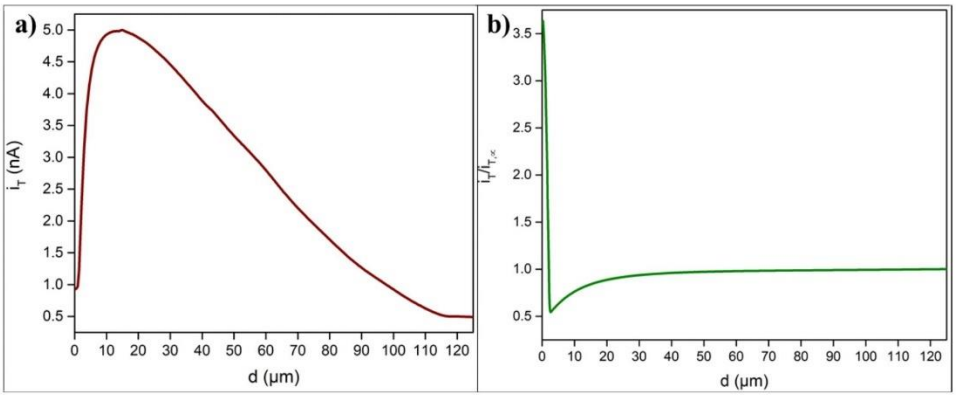

Figure S3: Approach curves recorded above $Mg_{17}Al_{12}$ surface using a) SG/TC mode with detection of H_2 at the tip, E_{tip} = 0 V vs. Ag/AgCl/NaCl and b) Feedback mode with $Fc(MeOH)_2$ as mediator at 1 mmol/L in ethanol, E_{tip}= 0.6 V vs. Ag/AgCl/NaCl. Tip radius = 12.5 µm, approach rate = 1 µm.s^{-1}.

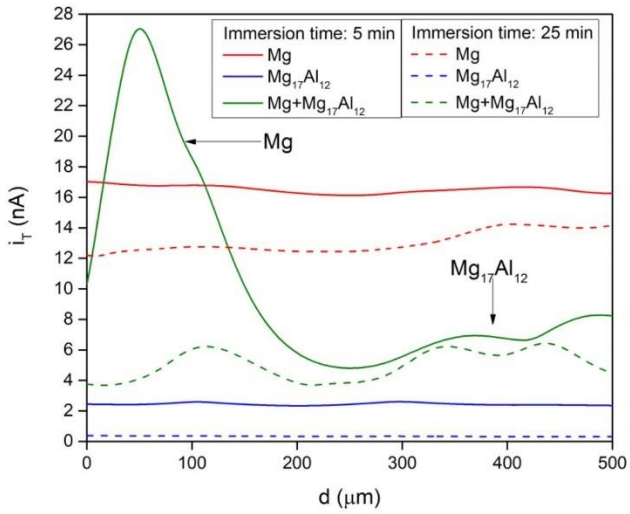

Figure S4: Line scan recorded above the surface of pure Mg, pure $Mg_{17}Al_{12}$ and $Mg+Mg_{17}Al_{12}$ after 5 minutes (solid line plot) and 25 minutes (dash line plot) of immersion in 0.06 M NaCl solution. Tip scan rate = 10 µm.s^{-1}.

SECM using feedback mode

Cyclic voltammetry in the bulk of $Fc(MeOH)_2$ solution was performed at the microelectrode without any influence of the substrate (Supplementary materials Figure S5). The steady state current appeared above 0.6 V/Ag and the oxidation of $Fc(MeOH)_2$ at the tip is limited by diffusion. Therefore, the tip was biased at 0.6 V vs. Ag in order to obtain complete diffusion-limited electrochemical oxidation of $Fc(MeOH)_2$ to $Fc(MeOH)_2^+$ in feedback mode.

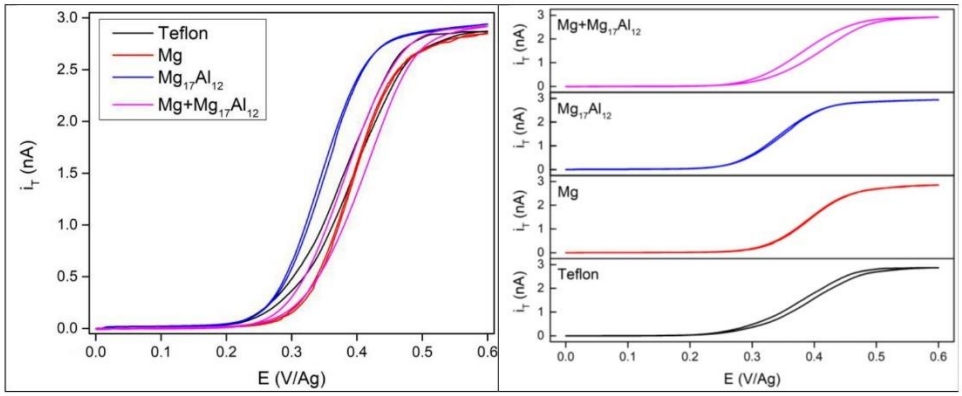

Figure S5: Cyclic voltammogram on the SECM probe in 1 mmol/L $Fc(MeOH)_2$ between 0 V/Ag and 0.6V/Ag above a Teflon surface, Mg, $Mg_{17}Al_{12}$ and $Mg+Mg_{17}Al_{12}$. Scan rate = 5 $mV.s^{-1}$.

The shape of the negative feedback approach curves in ethanol can be fitted with the model described by Cornut *et al.* [1]. This model suggests that the variation of the approach curve is directly related to the geometry of the UME and to the tip-substrate distance ($i_T/i_{T,\infty} = f$ (d, a, RG) where d the tip-substrate distance, a the UME radius and RG the ratio between the radius of the insulating sheath and the radius of the conductive disk; hence it is used to verify the RG ratio of the UME. Cornut *et al.* [2] developed an analytical approximation of kinetically limited feedback behavior, permitting the evaluation of the apparent heterogeneous rate constant k_{app}, between the

$Fc(MeOH)_2^+$ and the surface. Since we worked without supporting electrolyte, the migration must play a role in the mass transport of $Fc(MeOH)_2^+$. However, because the shape of the approach curves is close to the pure negative feedback, where the diffusion of $Fc(MeOH)_2$ is the limited step, we made the hypothesis that the migration can be neglected. By consequence, these theoretical curves have made it possible to evaluate the apparent heterogeneous rate constant k_{app} corresponding to the redox conversion of $Fc(MeOH)_2$ to $Fc(MeOH)_2^+$ on the substrate [2].

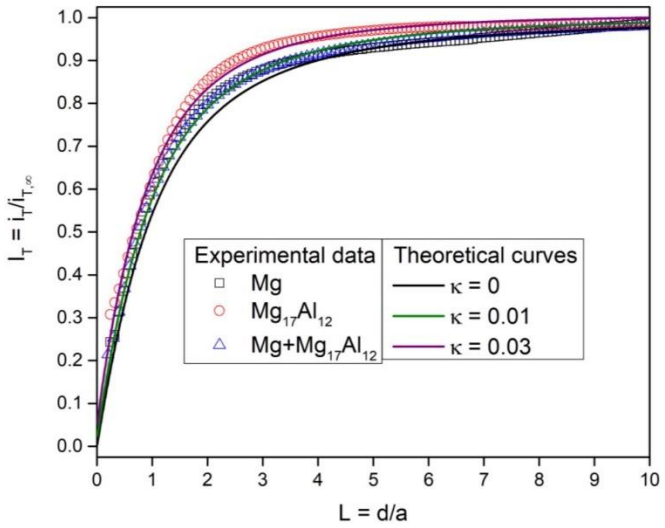

Figure S6: Z-approach curves (expressed as scatter line plot) recorded above pure Mg (□), pure $Mg_{17}Al_{12}$ (○) and $Mg+Mg_{17}Al_{12}$ (Δ) in feedback mode using $Fc(MeOH)_2$ as mediator and the theoretical curves (expressed as continuous line plot) calculated for RG = 7 and κ = 0 (—), κ = 0.01 (—) and κ = 0.03 (—). Approach rate = 1 µm.s^{-1}.

The experimental (scatter line plot) and the theoretical (continuous line plot) approach curves recorded above the surface of pure Mg, pure $Mg_{17}Al_{12}$ and $Mg+Mg_{17}Al_{12}$ are shown in Figure S6. Table S1 shows the values of the apparent heterogeneous rate constant k_{app} and the corrosion rate densities of the three materials. Tefashe *et al.* [3] showed that prolonging the immersion time of Mg in $Fc(MeOH)_2$ solution increases the thickness of the passivation layer and decreases the

apparent heterogeneous rate constant k_{app}. All the curves were recorded after an immersion time of 15 min. In our case, we never observed the positive feedback with $Fc(MeOH)_2$ in ethanol. This result suggests that a passivation layer is present even by using ethanol [4].

Table S1: The apparent heterogeneous rate constant k_{app} estimated from feedback approach curves fitting and the corrosion current densities (J_{corr}) in 0.6 mol/L NaCl solution for the three materials.

	Pure Mg	**Pure $Mg_{17}Al_{12}$**	**Mg+$Mg_{17}Al_{12}$**
k_{app} ($\times 10^{-3}$ cm.s^{-1})	0.49	1.54	0.51
J_{corr} (μA.cm^{-2})	558 [5]	5.3 [6] 2 [7]*	9500 [8]

* measurements were performed in 0.1 mol/L NaCl solution [7].

The k_{app} calculated for $Mg_{17}Al_{12}$ is greater than that on pure Mg while k_{app} (Mg+$Mg_{17}Al_{12}$) was similar to Mg because the approach curve is performed on the Mg part of the material. The corrosion current densities estimated from the Tafel plots varies as follow: $Mg_{17}Al_{12}$ < Mg < Mg+$Mg_{17}Al_{12}$ [5-8]. The fact that k_{app} value for $Mg_{17}Al_{12}$ is higher while the corrosion current density of $Mg_{17}Al_{12}$ is extremely lower than that of Mg indicates that the apparent heterogeneous rate constant is probably affected by the composition of the passivation layer as well as its thickness, which influence the diffusion of the mediator.

References

[1] S. Schumann. **The paths and strategies for increased magnesium applications in vehicles.** Mater. Sci. Forum, 488–489 (2005), pp. 1-8.

[2] C.H. Caceres. **Economical and environmental factors in light alloys automotive applications.** Metall. Mater. Trans. A, 38 (2007), pp. 1649-1662, 10.1007/s11661-007-9156-z

[3] R.E. Brown. **Magnesium recycling yesterday, today, tomorrow.** Recycling of Metals and Engineercd Materials (2013), pp. 1317-1329, 10.1002/9781118788073.ch115

[4] R.L. Edgar. **Global overview on demand and applications for magnesium alloys.** K.U. Kainer (Ed.), Magnesium Alloys and their Applications, Wiley-VCH Verlag GmbH & Co., KGaA, Weinheim, FRG (2006), pp. 1-8, 10.1002/3527607552.ch1

[5] G. Hanko, H. Antrekowitsch, P. Ebner. **Recycling automotive magnesium scrap.** Jom, 54 (2002), pp. 51-54, 10.1007/bf02701075

[6] A. Javaid, E. Essadiqi, S. Bell, B. Davis. **Literature review on magnesium recycling.** H.E. Friedrich, B.L. Mordike (Eds.), Magnesium Technology, Springer-Verlag, Berlin Heidelberg (2006), pp. 7-12, 10.1007/3-540-30812-1

[7] X. Xie, C. Ni, B. Wang, Y. Zhang, X. Zhao, L. Liu, B. Wang, W. Du. **Recent advances in hydrogen generation process via hydrolysis of Mg-based materials: a short review.** J. Alloy. Compd., 816 (2020), Article 152634, 10.1016/j.jallcom.2019.152634

[8] Z.H. Tan, L.Z. Ouyang, J.M. Huang, J.W. Liu, H. Wang, H.Y. Shao, M. Zhu. **Hydrogen generation via hydrolysis of Mg2Si.** J. Alloy. Compd., 770 (2019), pp. 108-115, 10.1016/j.jallcom.2018.08.122

[9] M. Ma, L. Yang, L. Ouyang, H. Shao, M. Zhu. **Promoting hydrogen generation from the hydrolysis of Mg-Graphite composites by plasma-assisted milling.** Energy, 167 (2019), pp. 1205-1211, 10.1016/j.energy.2018.11.029

[10] Z. Tan, L. Ouyang, J. Liu, H. Wang, H. Shao, M. Zhu. **Hydrogen generation by hydrolysis of Mg-Mg2Si composite and enhanced kinetics performance from introducing of MgCl2 and Si.** Int. J. Hydrogen Energy, 43 (2018), pp. 2903-2912, 10.1016/j.ijhydene.2017.12.163

[11] M. Huang, L. Ouyang, Z. Chen, C. Peng, X. Zhu, M. Zhu. **Hydrogen production via hydrolysis of Mg-oxide composites.** Int. J. Hydrogen Energy, 42 (2017), pp. 22305-22311, 10.1016/j.ijhydene.2016.12.099

[12] S.A. Pighin, G. Urretavizcaya, J.L. Bobet, F.J. Castro. **Nanostructured Mg for hydrogen production by hydrolysis obtained by MgH_2 milling and dehydriding.** J. Alloy. Compd., 827 (2020), Article 154000, 10.1016/j.jallcom.2020.154000

[13] L. Ouyang, W. Chen, J. Liu, M. Felderhoff, H. Wang, M. Zhu. **Enhancing the regeneration process of consumed NaBH4 for hydrogen storage.** Adv. Energy Mater., 7 (2017), p. 1700299, 10.1002/aenm.201700299

[14] Y. Zhu, L. Ouyang, H. Zhong, J. Liu, H. Wang, H. Shao, Z. Huang, M. Zhu. **Closing the loop for hydrogen storage: facile regeneration of NaBH4 from its hydrolytic product.** Angew. Chem. Int. Ed., 59 (2020), pp. 8623-8629, 10.1002/anie.201915988

[15] K. Chen, L. Ouyang, H. Zhong, J. Liu, H. Wang, H. Shao, Y. Zhang, M. Zhu. **Converting H+ from coordinated water into H− enables super facile synthesis of LiBH4.** Green Chem., 21 (2019), pp. 4380-4387, 10.1039/C9GC01897B

[16] S. Al Bacha, A.S. Awad, E. El Asmar, T. Tayeh, J.L. Bobet, M. Nakhl, M. Zakhour. **Hydrogen generation via hydrolysis of ball milled WE43 magnesium waste.** Int. J. Hydrogen Energy, 44 (2019), pp. 17515-17524, 10.1016/j.ijhydene.2019.05.123

[17] S. Al Bacha, S.A. Pighin, G. Urretavizcaya, M. Zakhour, F.J. Castro, M. Nakhl, J.L. Bobet. **Hydrogen generation from ball milled Mg alloy waste by hydrolysis reaction.** J. Power Sources, 479 (2020), Article 228711, 10.1016/j.jpowsour.2020.228711

[18] S. Al Bacha, S.A. Pighin, G. Urretavizcaya, M. Zakhour, M. Nakhl, F.J. Castro, J.L. Bobet. **Effect of ball milling strategy (milling device for scaling-up) on the hydrolysis performance of Mg alloy waste.** Int. J. Hydrogen Energy, 45 (2020), pp. 20883-20893, 10.1016/j.ijhydene.2020.05.214

[19] S. Al Bacha, A. Thienpont, M. Zakhour, M. Nakhl, J.L. Bobet. **Clean hydrogen production by the hydrolysis of magnesium-based material: effect of the hydrolysis solution.** J. Clean. Prod., 282 (2021), Article 124498, 10.1016/j.jclepro.2020.124498

[20] A. Kantürk Figen, B. Coşkuner Filiz. **Hydrogen production by the hydrolysis of milled waste magnesium scraps in nickel chloride solutions and nickel chloride added in Marmara Sea and Aegean Sea Water.** Int. J. Hydrogen Energy, 40 (2015), pp. 16169-16177, 10.1016/j.ijhydene.2015.07.170

[21] L.J. Liu, M. Schlesinger. **Corrosion of magnesium and its alloys.** Corros. Sci., 51 (2009), pp. 1733-1737, 10.1016/j.corsci.2009.04.025

[22] G.L. Song, A. Atrens. **Corrosion mechanisms of magnesium alloys.** Adv. Eng. Mater., 1 (1999), pp. 11-33.

[23] Y.-C. Zhao, M.-C. Zhao, R. Xu, L. Liu, J.-X. Tao, C. Gao, C. Shuai, A. Atrens. **Formation and characteristic corrosion behavior of alternately lamellar arranged α and β in as-cast AZ91 Mg alloy.** J. Alloy. Compd., 770 (2019), pp. 549-558, 10.1016/j.jallcom.2018.08.103

[24] E. Rocca, C. Juers, J. Steinmetz. **Corrosion behaviour of chemical conversion treatments on as-cast Mg–Al alloys: electrochemical and non-electrochemical methods.** Corros. Sci., 52 (2010), pp. 2172-2178, 10.1016/j.corsci.2010.02.036

[25] B.L. Mordike, T. Ebert. **Magnesium.** Mater. Sci. Eng.: A, 302 (2001), pp. 37-45, 10.1016/s0921-5093(00)01351-4

[26] R.-c Zeng, J. Zhang, W.-j Huang, W. Dietzel, K.U. Kainer, C. Blawert, W. Ke. **Review of studies on corrosion of magnesium alloys.** Trans. Nonferrous Met. Soc. China, 16 (2006), pp. s763-s771, 10.1016/s1003-6326(06)60297-5

[27] Z. Wen, C. Wu, C. Dai, F. Yang. **Corrosion behaviors of Mg and its alloys with different Al contents in a modified simulated body fluid.** J. Alloy. Compd., 488 (2009), pp. 392-399, 10.1016/j.jallcom.2009.08.147

[28] M. Esmaily, J.E. Svensson, S. Fajardo, N. Birbilis, G.S. Frankel, S. Virtanen, R. Arrabal, S. Thomas, L.G. Johansson. **Fundamentals and advances in magnesium alloy corrosion.** Prog. Mater. Sci., 89 (2017), pp. 92-193, 10.1016/j.pmatsci.2017.04.011

[29] Y.-l Cheng, T.-w Qin, H.-m Wang, Z. Zhang. **Comparison of corrosion behaviors of AZ31, AZ91, AM60 and ZK60 magnesium alloys.** Trans. Nonferrous Met. Soc. China, 19 (2009), pp. 517-524, 10.1016/s1003-6326(08)60305-2

[30] G. Song, A. Atrens, X. Wu, B. Zhang. **Corrosion behaviour of AZ21, AZ501 and AZ91 in sodium chloride.** Corros. Sci., 40 (1998), pp. 1769-1791, 10.1016/s0010-938x(98)00078-x

[31] A. Pardo, M.C. Merino, A.E. Coy, F. Viejo, R. Arrabal, S. Feliú. **Influence of microstructure and composition on the corrosion behaviour of Mg/Al alloys in chloride media.** Electrochim. Acta, 53 (2008), pp. 7890-7902, 10.1016/j.electacta.2008.06.001

[32] O. Lunder, J.E. Lein, T.K. Aune, K. Nisancioglu. **The role of Mg17Al12 phase in the corrosion of Mg alloy AZ91.** Corrosion, 45 (1989), pp. 741-748, 10.5006/1.3585029

[33] S.A. Salman, R. Ichino, M. Okido. **A comparative electrochemical study of AZ31 and AZ91 magnesium alloy.** Int. J. Corrosion, 2010 (2010), pp. 1-7, 10.1155/2010/412129

[34] L. Wang, T. Shinohara, B.-P. Zhang. **Electrochemical behaviour of AZ61 magnesium alloy in dilute NaCl solutions.** Mater. Des., 33 (2012), pp. 345-349, 10.1016/j.matdes.2011.02.019

[35] A. Samaniego, I. Llorente, S. Feliu. **Combined effect of composition and surface condition on corrosion behaviour of magnesium alloys AZ31 and AZ61.** Corros. Sci., 68 (2013), pp. 66-71, 10.1016/j.corsci.2012.10.034

[36] I.B. Singh, M. Singh, S. Das. **A comparative corrosion behavior of Mg, AZ31 and AZ91 alloys in 3.5% NaCl solution.** J. Magnes. Alloy., 3 (2015), pp. 142-148, 10.1016/j.jma.2015.02.004

[37] H. Feng, S. Liu, Y. Du, T. Lei, R. Zeng, T. Yuan. **Effect of the second phases on corrosion behavior of the Mg-Al-Zn alloys.** J. Alloy. Compd., 695 (2017), pp. 2330-2338, 10.1016/j.jallcom.2016.11.100

[38] M.C. Zhao, P.J. Uggowitzer, M. Liu, P. Schmutz, G. Song, A. Atrens. **Corrosion of AZ91 - influence of the β-phase morphology.** Mater. Sci. Forum, 618–619 (2009), pp. 473-478, 10.4028/www.scientific.net/MSF.618-619.473

[39] A. Atrens, G.-L. Song, M. Liu, Z. Shi, F. Cao, M.S. Dargusch. **Review of recent developments in the field of magnesium corrosion.** Adv. Eng. Mater., 17 (2015), pp. 400-453, 10.1002/adem.201400434

[40] C. Ubeda, G. Garces, P. Adeva, I. Llorente, G.S. Frankel, S. Fajardo. **The role of the beta-Mg17Al12 phase on the anomalous hydrogen evolution and anodic dissolution of AZ magnesium alloys.** Corros. Sci., 165 (2020), Article 108384, 10.1016/j.corsci.2019.108384

[41] S. Al Bacha, I. Aubert, O. Devos, M. Zakhour, M. Nakhl, J.L. Bobet. **Corrosion of pure and milled Mg17Al12 in "model" seawater solution.** Int. J. Hydrogen Energy, 45 (2020), pp. 15805-15813, 10.1016/j.ijhydene.2020.04.030

[42] S. Al Bacha, I. Aubert, M. Zakhour, M. Nakhl, J.L. Bobet. **Hydrolysis properties, corrosion behavior and microhardness of AZ91 "model" alloys.** J. Alloy. Compd., 845 (2020), Article 156283, 10.1016/j.jallcom.2020.156283

[43] Gv Baril, C. Blanc, M. Keddam, N. Pébère. **Local electrochemical impedance spectroscopy applied to the corrosion behavior of an AZ91 magnesium alloy.** J. Electrochem. Soc., 150 (2003), pp. B488-8, 10.1149/1.1602080

[44] G. Galicia, N. Pébère, B. Tribollet, V. Vivier. **Local and global electrochemical impedances applied to the corrosion behaviour of an AZ91 magnesium alloys.** Corros. Sci., 51 (2009), pp. 1789-1794, 10.1016/j.corsci.2009.05.005

[45] G. Williams, H. Neil McMurray. **Localized corrosion of magnesium in chloride-containing electrolyte studied by a scanning vibrating electrode technique.** J. Electrochem. Soc., 155 (2008), p. C340, 10.1149/1.2918900

[46] M. Jönsson, D. Thierry, N. LeBozec. **The influence of microstructure on the corrosion behaviour of AZ91D studied by scanning Kelvin probe force microscopy and scanning Kelvin probe.** Corros. Sci., 48 (2006), pp. 1193-1208, 10.1016/j.corsci.2005.05.008

[47] P. Dauphin-Ducharme, C. Kuss, D. Rossouw, N.A. Payne, L. Danis, G.A. Botton, J. Mauzeroll. **Corrosion product formation monitored using the feedback mode of scanning electrochemical microscopy with carbon microelectrodes.** J. Electrochem. Soc., 162 (2015), pp. C677-C683, 10.1149/2.0701512jes

[48] M.V. Mirkin, W. Nogala, J. Velmurugan, Y. Wang. **Scanning electrochemical microscopy in the 21st century. Update 1: Five years after.** Phys. Chem. Chem. Phys., 13 (2011), pp. 21196-21212, 10.1039/c1cp22376c

[49] G. Wittstock, M. Burchardt, S.E. Pust, Y. Shen, C. Zhao. **Scanning electrochemical microscopy for direct imaging of reaction rates.** Angew. Chem. Int. Ed. Engl., 46 (2007), pp. 1584-1617, 10.1002/anie.200602750

[50] D. Polcari, P. Dauphin-Ducharme, J. Mauzeroll. **Scanning electrochemical microscopy: a comprehensive review of experimental parameters from 1989 to 2015.** Chem. Rev., 116 (2016), pp. 13234-13278, 10.1021/acs.chemrev.6b00067

[51] N.A. Payne, L.I. Stephens, J. Mauzeroll. **The application of scanning electrochemical microscopy to corrosion research.** Corrosion, 73 (2017), pp. 759-780, 10.5006/2354

[52] G.S. Frankel, A. Samaniego, N. Birbilis. **Evolution of hydrogen at dissolving magnesium surfaces.** Corros. Sci., 70 (2013), pp. 104-111, 10.1016/j.corsci.2013.01.017

[53] J.M. Huang, R.M. Duan, L.Z. Ouyang, Y.J. Wen, H. Wang, M. Zhu. **The effect of particle size on hydrolysis properties of Mg3La hydrides.** Int. J. Hydrogen Energy, 39 (2014), pp. 13564-13568, 10.1016/j.ijhydene.2014.04.024

[54] E. Alasmar, I. Aubert, A. Durand, M. Nakhl, M. Zakhour, E. Gaudin, J.L. Bobet. **Hydrogen generation from Mg NdNiMg15 composites by hydrolysis reaction.** Int. J. Hydrogen Energy, 44 (2019), pp. 523-530, 10.1016/j.ijhydene.2018.10.233

[55] S. Al Bacha, M. Zakhour, M. Nakhl, J.L. Bobet. **Effect of ball milling in presence of additives (Graphite, $AlCl_3$, $MgCl_2$ and NaCl) on the hydrolysis performances of $Mg_{17}Al_{12}$.** Int. J. Hydrogen Energy, 45 (2020), pp. 6102-6109, 10.1016/j.ijhydene.2019.12.162

[56] D. Zigah, E. Lojou, A. Poulpiquet. **Micro- and nanoscopic imaging of enzymatic electrodes: a review.** ChemElectroChem, 6 (2019), pp. 5524-5546, 10.1002/celc.201901065

[57] F. Zhou, P.R. Unwin, A.J. Bard. **Scanning electrochemical microscopy. 16. Study of second-order homogeneous chemical reactions via the feedback and generation/collection modes.** J. Phys. Chem., 96 (2002), pp. 4917-4924, 10.1021/j100191a036

[58] D. Filotás, B.M. Fernández-Pérez, L. Nagy, G. Nagy, R.M. Souto. **A novel scanning electrochemical microscopy strategy for the investigation of anomalous hydrogen evolution from AZ63 magnesium alloy.** Sens. Actuators B: Chem., 308 (2020), Article 127691, 10.1016/j.snb.2020.127691

[59] U.M. Tefashe, M.E. Snowden, P.D. Ducharme, M. Danaie, G.A. Botton, J. Mauzeroll. **Local flux of hydrogen from magnesium alloy corrosion investigated by scanning electrochemical microscopy.** J. Electroanal. Chem., 720–721 (2014), pp. 121-127, 10.1016/j.jelechem.2014.03.002

[60] M. Grosjean, M. Zidoune, J. Huot, L. Roue. **Hydrogen generation via alcoholysis reaction using ball-milled Mg-based materials.** Int. J. Hydrogen Energy, 31 (2006), pp. 1159-1163, 10.1016/j.ijhydene.2005.10.001

[61] H. Hu, X. Nie, Y. Ma. **Corrosion and surface treatment of magnesium alloys.** F. Czerwinski (Ed.), Magnesium Alloys-Properties in Solid and Liquid States, IntechOpen (2014), pp. 67-108, 10.5772/58929

[62] A.J. Bard, G. Denuault, C. Lee, D. Mandler, D.O. Wipf. **Scanning electrochemical microscopy - a new technique for the characterization and modification of surfaces.** Acc. Chem. Res., 23 (2002), pp. 357-363, 10.1021/ar00179a002

[63] S. Al Bacha, A. Desmedt, M. Zakhour, M. Nakhl, J.L. Bobet. **Mechanism of hydrogen formation during the corrosion of $Mg_{17}Al_{12}$.** Electrochem. Commun., 119 (2020), Article 106813, 10.1016/j.elecom.2020.106813

[64] J. Kwak, A.J. Bard. **Scanning electrochemical microscopy. Theory of the feedback mode.** Anal. Chem., 61 (2002), pp. 1221-1227, 10.1021/ac00186a009

[65] R. Cornut, C. Lefrou. **A unified new analytical approximation for negative feedback currents with a microdisk SECM tip.** J. Electroanal. Chem., 608 (2007), pp. 59-66, 10.1016/j.jelechem.2007.05.007

[66] P. Dauphin-Ducharme, J. Mauzeroll. **Surface analytical methods applied to magnesium corrosion.** Anal. Chem., 87 (2015), pp. 7499-7509, 10.1021/ac504576g

[67] S.-L. Li, H.-M. Lin, J.-Y. Uan. **Production of an Mg/Mg2Ni lamellar composite for generating H2 and the recycling of the post-H2 generation residue to nickel powder.** Int. J. Hydrogen Energy, 38 (2013), pp. 13520-13528, 10.1016/j.ijhydene.2013.08.051

[68] E. Mena-Morcillo. **In situ investigation of the initial stages of AZ91D magnesium alloy biodegradation in simulated body fluid.** Int. J. Electrochem. Sci., 13 (2018), pp. 5141-5150, 10.20964/2018.06.47

[69] T. Tayeh, A.S. Awad, M. Nakhl, M. Zakhour, J.F. Silvain, J.L. Bobet. **Production of hydrogen from magnesium hydrides hydrolysis.** Int. J. Hydrogen Energy, 39 (2014), pp. 3109-3117, 10.1016/j.ijhydene.2013.12.082

[70] S. Palit. **Recent advances in corrosion science: a critical overview and a deep comprehension.** B. Kharisov (Ed.), Direct Synthesis of Metal Complexes, Elsevier (2018), pp. 379-411, 10.1016/b978-0-12-811061-4.00011-6

[71] A.D. Südholz, N.T. Kirkland, R.G. Buchheit, N. Birbilis. **Electrochemical properties of intermetallic phases and common impurity elements in magnesium alloys.** Electrochem. Solid-State Lett., 14 (2011), pp. C5-C7, 10.1149/1.3523229